

Non-hyperbolicity in large-scale dynamics of a chaotic system

Caroline Wormell*

June 4, 2022

Abstract

Many important high-dimensional dynamical systems exhibit complex chaotic behaviour. Their complexity means that their dynamics are necessarily comprehended under strong reducing assumptions. It is therefore important to have a clear picture of these reducing assumptions' range of validity. The highly influential chaotic hypothesis of Gallavotti and Cohen states that the large-scale dynamics of high-dimensional systems are effectively hyperbolic, which implies many felicitous statistical properties. We demonstrate, contrary to the chaotic hypothesis, the existence of non-hyperbolic large-scale dynamics in a mean-field coupled system. To do this we reduce the system to its thermodynamic limit, which we approximate numerically with a Chebyshev Galerkin transfer operator discretisation. This enables us to obtain a high precision estimate of a homoclinic tangency, implying a failure of hyperbolicity. Robust non-hyperbolic behaviour is expected under perturbation. As a result, the chaotic hypothesis should not be assumed to hold in all systems, and a better understanding of the domain of its validity is required.

1 Introduction

By and large, complex systems have chaotic dynamics on a substantial set of parameters. The most salient example of this is the Earth's climate system. The chaotic dynamics of such systems are almost universally too complicated to treat from rigorous first principles, and so general simplifying principles are therefore necessary to understand the system's most important components. When the system is spatially structured, such as in climate models, these components are often the dynamics taking place on large spatial scales.

The paradigmatic subclass of chaotic systems are uniformly hyperbolic systems, which have a uniform splitting between expanding and contracting directions [10]. Because of their simple geometry, these systems are very amenable to

*Laboratoire de Probabilités, Statistique et Modélisation (LPSM), Sorbonne Université, Université de Paris
email: wormell@lpsm.paris

study. Without hyperbolicity assumptions, however, our rigorous knowledge of multidimensional chaotic systems is meagre. This is a major problem, because real-life examples of hyperbolic chaotic dynamics are very rare [24].

Nonetheless, it is conjectured that, when considered at large scales, typical chaotic dynamics resolve as hyperbolic [16]:

Hypothesis 1 (Gallavotti–Cohen chaotic hypothesis [17, 18]) *The macroscopic dynamics of a (high-dimensional) chaotic system on its attractor can be regarded as a transitive hyperbolic (“Anosov”) evolution.*

In fact, many “nice” statistical properties possessed by hyperbolic systems are also found in the macroscopic-scale dynamics of certain large non-hyperbolic systems. These properties include existence of physical invariant measures, exponential mixing and large deviation laws [25, 27]. Hypothesised mechanisms include emergent stochastic effects in coupled systems [46, 47], matching of topological equivalency classes between different subsystems under perturbations [47], and generic distribution of singularities in the system [38]. The chaotic hypothesis suggests that general high-dimensional chaotic systems may be studied using techniques developed for hyperbolic systems, an idea which has been much taken up in the geophysics literature [19, 28].

However, seeming counter-examples to this phenomena arise when considering the response of the physical invariant measure to dynamical perturbations. Hyperbolic systems are known to have a so-called “linear response”, that is to say their statistics vary differentiably when a parameter of the chaotic system is varied [37]: many smooth non-uniformly hyperbolic systems on the other hand fail to have a linear, or even a continuous response [1, 3]. While in many geophysical systems linear response theory has been successful [5, 9, 29, 14, 36, 26], certain ones appear to respond non-differentiably to perturbations [13, 12]. Nonetheless, it is arguable that linear response falls outside the scope of the chaotic hypothesis, because the hypothesis only pertains to individual systems, whereas a linear response is a property of a family of systems [46].

In recent times, linear response behaviour of complex chaotic systems has been investigated through the increasingly popular model of mean-field coupled maps. These are systems composed of many chaotic subsystems that interact with each other through a mean-field [20]. They are a subset of globally-coupled maps [11]. As the number of subsystems tends to infinity, the large-scale behaviour of these systems can be described by a so-called thermodynamic limit system [35, 22]. These limit systems may exhibit non-trivial dynamics [22, 41, 21]. With certain hyperbolic subsystems and sufficiently weak couplings, linear responses have been proven to exist in thermodynamic limit systems [42, 15]. On the other hand, [47] presented a mean-field coupled system whose thermodynamic limit’s response to perturbations appeared to be non-smooth. This was argued to be the result of an apparent structural similarity between the thermodynamic limit and the non-hyperbolic Hénon map, for which linear response fails.

The goal of this paper is to furnish an explicit example of non-hyperbolicity in a thermodynamic limit system similar to that of [47]. The non-hyperbolic

limit system we present has a homoclinic orbit whose stable and unstable directions are tangent to each other, a phenomenon which is definitionally excluded in hyperbolic dynamics. Because the thermodynamic limit system's attractor contains this homoclinic tangency, it violates the Hypothesis 1.

Apart from self-evidently demonstrating non-hyperbolicity for a single limit system, the existence of a generic homoclinic tangency also suggests so-called wild dynamical phenomena on a generic set of nearby limit systems. Examples include the existence of infinitely many sinks (*i.e.* stable periodic orbits) [31, 6, 7], or more relevantly, of other tangencies between stable or unstable manifolds, *i.e.* the persistence of non-hyperbolic behaviour [34]. Thus, the homoclinic tangency we obtained for one system would imply a violation of the chaotic hypothesis for a large set of nearby systems.

Our evidence for the homoclinic tangency is numerical. To approximate the infinite-dimensional limit system, we will apply Chebyshev Galerkin discretisations for the transfer operators that describe the thermodynamic limit [45, 4], using the software package `Poltergeist.jl` [44]. Such discretisations are very accurate and efficient in approximating such objects. To obtain the homoclinic tangency in this system we will use a shooting method. With these methods the homoclinic tangency is estimated to a very high accuracy. This furnishes very strong evidence of its existence.

The paper is structured as follows. In Section 2, the mean-field coupled system and its thermodynamic limit are presented, and in Section 3 the mathematical objects required to describe a homoclinic tangency are introduced. In Sections 4-5 numerical methods are presented: first the scheme to approximate the thermodynamic limit map, and then the method to find the homoclinic tangency. The results are presented in Section 6 and in Section 7 implications and further directions are discussed.

2 Model

2.1 Mean-field system

We introduce a mean-field system, similar to those proposed in [47], composed of $M \gg 1$ one-dimensional chaotic subsystems $q^{(j)}$ coupled together via a mean field Φ . These chaotic subsystems $q^{(j)} \in [-1, 1]$ each evolve according to smooth, individually hyperbolic (in fact uniformly-expanding) chaotic dynamics

$$q_{n+1}^{(j)} = f_{t\Phi_n}(q_n^{(j)}), \quad (1)$$

modulated by a mean field

$$\Phi_n = \frac{1}{M} \sum_{j=1}^M q_n^{(j)} \quad (2)$$

and a fixed parameter $t \geq 0$ which determines the strength of the coupling.

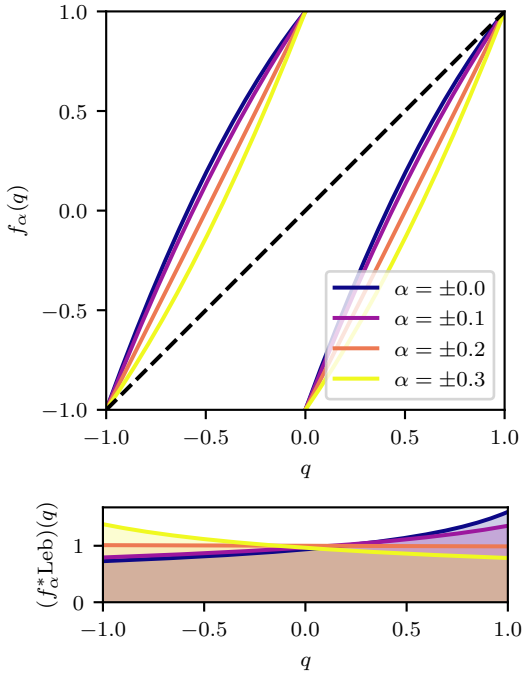


Figure 1: Top: graph of the microscopic maps f_α for some representative values of α .

Bottom: for various α , the action of f_α on Lebesgue measure: that is, $\mathcal{L}_\alpha 1$ for various values of α . Note that because the Lebesgue measure of the domain $[-1, 1]$ is 2, these measures are actually *twice* a probability measure.

For the subsystem dynamics we chose

$$f_\alpha(q_n) = \mathfrak{d}(x) + g(\alpha) * (1 - \mathfrak{d}(x)^2),$$

where $\mathfrak{d}(q) := 2q - \text{sign } q$ is the doubling map on $[-1, 1]$, and

$$g(\alpha) = \frac{3}{16} \cos 8\alpha \in \left(-\frac{3}{16}, \frac{3}{16}\right).$$

1) are piecewise analytic maps of the interval, with two full branches. They are uniformly expanding, with each $|f'_\alpha| \geq \frac{5}{4} > 1$.

Dynamically, the choice of f (in particular of g) encourages the $q^{(j)}$ to take higher values (increasing Φ_{n+1}) for $t\Phi_n$ close to zero, and towards $q = -1$ for $t\Phi_n$ appropriately far from zero. This induces quasi-unimodal dynamics in the mean position of the $q^{(j)}$'s for $t \lesssim 3$.

2.2 Thermodynamic limit reduction

To reduce this system to its macroscopic components, it is possible to use the exchangeability of the $q^{(j)}$ to write the system (1-2) in terms of the empirical measure $\mu_n = \frac{1}{M} \sum_{j=1}^M \delta_{q_n^{(j)}}$:

$$\mu_{n+1} = (f_{t\Phi_n})_* \mu_n,$$

$$\Phi_n = \int_{-1}^1 q \, d\mu_n(q),$$

where $(f_{t\Phi_n})_*$ is the push-forward of $f_{t\Phi_n}$. Statistics of the $q_n^{(j)}$ can then be recovered through averages over μ_n . As the number of subsystems $M \rightarrow \infty$ we can expect the discrete empirical measures μ_n to converge to probability distributions with appropriately smooth Lebesgue densities [22]. In a mild abuse of notation, we will write these density functions also as μ_n . We can thus rewrite our dynamics as

$$\mu_{n+1} = \mathcal{L}_{t\Phi_n} \mu_n, \tag{3}$$

$$\Phi_n = \varphi[\mu_n] \tag{4}$$

where \mathcal{L}_α is the transfer operator of f_α , with explicit expression

$$(\mathcal{L}_\alpha h)(x) = \sum_{y \in f_\alpha^{-1}(x)} \frac{h(y)}{f'_\alpha(y)}, \tag{5}$$

and the functional $\varphi[\mu] = \int q \mu(q) \, dq$.

The system (3-4) can be reformulated as a delay equation in mean field Φ_n [47], but can more simply be solved as a function of the measure distribution

$$\mu_{n+1} = F_t(\mu_n) := \mathcal{L}_{t\varphi[\mu_n]} \mu_n. \tag{6}$$

Because we have assumed that μ_n are smooth, absolutely continuous probability measures, we assume that the dynamics takes place within the space U of positive, twice-differentiable densities that integrate to 1 on $[0, 1]$. However, we can use the uniform analyticity of the maps f_α to further restrict the thermodynamic limit dynamics F_t to act on a scale of function spaces on which it has relatively nice compactness properties.

2.3 Hardy function spaces

The Banach spaces we use are Hardy spaces H_ρ , $\rho > 0$ of analytic functions. For small enough ρ the sets $H_\rho \cap U$ form attracting¹ invariant sets of the F -dynamics on U .

¹The attractiveness we expect because the Hardy spaces H_ρ are dense in the space of twice-differentiable functions C^2 , and the differentials of iterates of F_t can be shown to be quasi-compact in C^2 with essential spectral radius smaller than 1, and compact in H_ρ . In other words, the differentials of F_t contract C^2 onto H_ρ even when they are expanding in H_ρ .

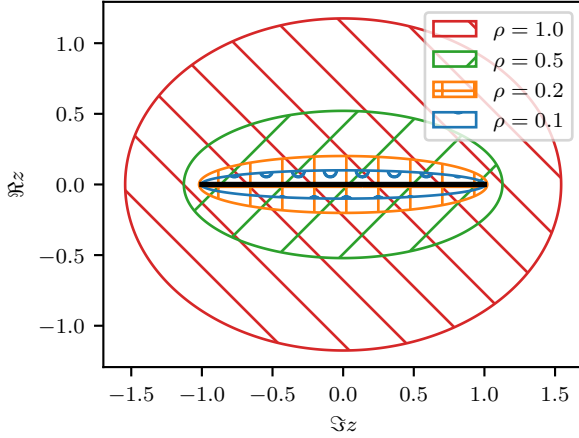


Figure 2: Bernstein ellipses for various parameters ρ .

The domain of a function in H_ρ is the Bernstein ellipse E_ρ :

$$[-1, 1] \subseteq E_\rho = \cos([0, \pi] + i[-\rho, \rho]) \subset \mathbb{C}.$$

These are ellipses in the complex plane centred at 0 with semi-axes $\cosh \rho > 1$ and $\sinh \rho > 0$: a range are plotted in Figure 2. The Hardy space H_ρ is composed of continuous complex functions on E_ρ which are analytic on its interior, equipped with the supremum norm

$$\|h\|_\rho = \sup_{z \in E_\rho} |h(z)|.$$

As an edge case, the H_0 norm is simply the L^∞ norm on $[-1, 1]$.

Now, because of its definition through function composition (5), the transfer operator \mathcal{L}_α is bounded from larger Hardy spaces into smaller ones [4].

In particular, if $0 < R \leq R_{\max} := 0.5$ and $r \geq 0.93R$, one can show that all $\alpha \in \mathbb{R}$ that $f_\alpha^{-1}(E_R)$ is a subset of E_r . Hence, if $h \in H_r$,

$$\begin{aligned} \|\mathcal{L}_\alpha h\|_R &= \sup_{z \in E_R} \left| \sum_{w \in f_\alpha^{-1}(z)} \frac{h(w)}{f'_\alpha(w)} \right| \\ &\leq 2 \sup_{w \in f_\alpha^{-1}(E_R)} \left| \frac{h(w)}{f'_\alpha(w)} \right| \\ &\leq \frac{2 \sup_{w \in E_r} |h(w)|}{\inf_{w \in f_\alpha^{-1}(E_R)} |f'_\alpha(w)|} \\ &\leq 1.85 \|h\|_r, \end{aligned} \tag{7}$$

In particular, every \mathcal{L}_α is uniformly bounded as an operator $H_r \rightarrow H_R$ for $R \in (0, R_{\max}]$ and $r \geq 0.93R_{\max}$.

This means \mathcal{L}_α is bounded as an endomorphism on both H_r and H_R since $\|\cdot\|_r \leq \|\cdot\|_R$ for $r \leq R$. Better than this, inclusions between Hardy spaces of different parameters are very strongly compact, in fact nuclear. This is a simple fact falling out of Fourier analysis [43]. Hence as an endomorphism on H_r , the transfer operator \mathcal{L}_α has the same strong uniform compactness properties.

On these Hardy spaces, the transfer operator also has a very nice perturbation theory. It is a standard fact of complex analysis the differentiation operator ∂_q and its iterates ∂_q^k are also bounded as operators $H_R \rightarrow H_r$ for any $r < R$. A particular consequence of this is that, since the derivatives of the transfer operator with respect to dynamical perturbations, that is $\frac{d^k \mathcal{L}_\alpha}{d\alpha^k}$, can be expressed as linear combinations of $\partial_q^j \mathcal{L}_\alpha$, $j \leq k$ [40, Section 2.3], these derivatives are also bounded as operators $H_r \rightarrow H_r$. In our setting, the map $\alpha \mapsto \mathcal{L}_\alpha$ is therefore a C^∞ function $\mathbb{R} \rightarrow L(H_r, H_r)$ for appropriate positive choices of $r < 0.93R_{\max}$. This justifies the perturbation theory used in the rest of the paper.

3 Manifolds and tangencies

It is now necessary to define the manifold structure of F_t , which will allow us to speak to its (non-)hyperbolicity.

Let us generally suppose simply that we have a dynamical system F acting on an affine subspace M of a Banach space with tangent space TM . The stable manifold of a point $x \in M$ is the set of points near x whose forward orbits converge to that of x :

$$\mathcal{V}_x^s = \{y \in M : \lim_{n \rightarrow \infty} d_M(F^n x, F^n y) = 0\},$$

where d_M is the metric on M . The local stable manifold of x is the set of such points which additionally do not leave some ϵ -neighbourhood of x :

$$\mathcal{V}_x^{s,\epsilon} = \{y \in M : \lim_{n \rightarrow \infty} d_M(F^n x, F^n y) = 0, \sup_{n \in \mathbb{N}} d_M(F^n x, F^n y) \leq \epsilon\} \subset \mathcal{V}_x^s.$$

Similarly, when F is a diffeomorphism, the unstable manifold of x is the set of points with *backward* orbits converging to that of x :

$$\mathcal{V}_x^u = \{y \in M : \lim_{n \rightarrow \infty} d_M(F^{-n} x, F^{-n} y) = 0\}.$$

We can extend these notions of stable and unstable manifolds onto the tangent bundles. For $x \in M$ let $D_x F : TM \rightarrow TM$ be the differential of F , that is to say that for all tangent vectors $v \in TM$

$$F(x + \epsilon v) = F(x) + \epsilon D_x F v + \mathcal{O}(\epsilon^2).$$

The *stable subspace* at x , $E_x^s \subseteq TM$, is then the set of tangent vectors at x which converge to zero under the action of T :

$$E_x^s = \{v \in T_x M : \lim_{n \rightarrow \infty} D_x F^n v = 0\},$$

where $D_x F$ is the Jacobian (or differential) of F . Similarly the *unstable subspace* at x is given as

$$E_x^u = \{v \in T_x M : \lim_{n \rightarrow \infty} D_x F^{-n} v = 0\}.$$

These are respectively tangent to stable and unstable manifolds [10].

Because our limiting dynamics F_t given in (6) are not a diffeomorphisms,² the unstable manifolds and subspaces are ill-defined. However, it is possible to define the unstable manifold (resp. subspace) of a backward orbit $(x_{-n})_{n \in \mathbb{N}}$. If x_* is a fixed point then for convenience we will define $\mathcal{V}_{x_*}^u$ (resp. $E_{x_*}^u$) to be the unstable manifold (resp. subspace) of the orbit $x_{-n} \equiv x_*$.

If x is a fixed point, then \mathcal{V}_x^s are the set of points with orbits converging to x , and \mathcal{V}_x^u are the set of points with orbits emanating from x ; furthermore, provided that the differential $D_x F$ is hyperbolic (*i.e.* its spectrum is bounded away from the unit circle), E_x^s is the span of the stable eigenspaces and E_x^u the span of the unstable eigenspaces.

A separation between unstable and stable subspaces are key properties of most well-behaved chaotic systems. A system is *uniformly hyperbolic* if at every point $x \in M$ the tangent space has an F -invariant splitting $T_x M = E_x^s \oplus E_x^u$, and there are constants $c > 0$, $\lambda < 1$ such that for all $x \in M$,

$$\begin{aligned} \|D_x F^n|_{E_x^s}\| &\leq c\lambda^n, \\ \|D_x F^{-n}|_{E_x^u}\| &\leq c\lambda^n. \end{aligned}$$

According to Hypothesis 1, the F_t are supposedly transitive and (uniformly) hyperbolic on their respective attractors. These two conditions together are the Axiom A of Smale [10].

One generic mechanism to generate non-hyperbolic dynamics is via homoclinic tangencies. A *homoclinic tangency* in a map $F : M \rightarrow M$ is a hyperbolic fixed point p of F together with a different point $q \in \mathcal{V}_p^u \cap \mathcal{V}_p^s$ such that \mathcal{V}_p^u and \mathcal{V}_p^s are tangent at q [39]. In particular, the stable and unstable subspaces E_q^s and E_q^u have non-trivial intersection, implying non-hyperbolicity of the given map F .

It is easy enough to show that a homoclinic tangency is equivalent to having that $q \in \mathcal{V}_p^u$ with $\lim_{n \rightarrow \infty} F^n(q) = p$ and $\lim_{n \rightarrow \infty} \|D_q F^n|_{E_q^u}\| \rightarrow 0$, because the stable subspaces E_q^s vary continuously at p since it is a hyperbolic fixed point.

4 Spectral methods

In Section 2.3 we discussed the strong compactness and regularity properties of F_t in certain Hardy spaces. This allows us to very effectively approximate the dynamics of the F_t and invariant manifolds on the computer, through projection onto a basis of Chebyshev polynomials.

²Note that, at the expense of complicating the perturbation theory, we could make the maps F_t closer to diffeomorphisms by adding hidden dynamics $r_{n+1} = \frac{1}{2}(r_n + \mathbf{1}_{q_n > 1/2}) \in [0, 1]$ and choosing F_t to act on an appropriate subset of a Triebel space [2].

The Chebyshev polynomials $T_k, k = 0, 1, \dots$ are a polynomial family orthogonal in $L^2_{\text{Cheb}} := L^2([-1, 1], dx/\sqrt{1-x^2})$:

$$\int_{-1}^1 T_k(x) T_j(x) \frac{dx}{\sqrt{1-x^2}} = w_k \delta_{jk},$$

where $w_k := \frac{\pi(1+\delta_{0k})}{2}$. They have explicit expression

$$T_k(x) = \cos(k \cos^{-1} x),$$

from which falls out a natural connection to Fourier series under the one-to-two transformation $x = \cos \theta$.

Chebyshev approximation is just about optimally adapted to this compact inclusion. Let P_n be the L^2_{Cheb} orthogonal projection onto the first n Chebyshev polynomials. It is a standard result that if $C_{R-r} := (1 - e^{-(R-r)})^{-1}$ then for $0 \leq r < R$ we have [43]

$$\|(I - P_n)h\|_r \leq C_{R-r} e^{-(R-r)n} \|h\|_R. \quad (8)$$

On the other hand, from (7) we know that for $r \leq 0.93R$, $R \in (0, R_{\max}]$

$$\sup_{\alpha \in \mathbb{R}} \|\mathcal{L}_\alpha h\|_r \leq 0.85 \|h\|_R.$$

From these two equations we therefore know that for such r, R and for all $\alpha \in \mathbb{R}$,

$$\|(I - P_n)\mathcal{L}_\alpha\|_r \leq \|I - P_n\|_{r \rightarrow R} \|\mathcal{L}_\alpha\|_{R \rightarrow r} \leq 0.85 C_{R-r} e^{-(R-r)n}.$$

This implies that the so-called Chebyshev Galerkin approximation $P_n \mathcal{L}_\alpha$ of the transfer operator \mathcal{L}_α converges exponentially to the true operator, and thus so do its spectrum and eigenvalues [4]. This can also be extended to more complex functions of \mathcal{L}_α such as the differential of F_t defined in (9) below.

The Galerkin approximations $P_n \mathcal{L}_\alpha$ are finite-dimensional, and such operators can be easily computed to high accuracy and faithfully represented using the theory of Chebyshev series [43]. In particular, if we represent the image of the projection P_n in the Chebyshev basis $\{T_k\}_{k=0, \dots, n-1}$, then the finite-rank operators $P_n \mathcal{L}_\alpha|_{P_n}$ can be represented as $n \times n$ matrixs in this basis, with entries

$$L_\alpha^{jk} = w_k^{-1} \int_{-1}^1 (\mathcal{L} - \alpha T_k)(x) T_j(x) \frac{dx}{\sqrt{1-x^2}}.$$

These entries can be computed very efficiently by interpolating the action of the operator on a sufficiently large number of Chebyshev points. Indeed, we have exponential convergence in the number of interpolating points N [43]

$$L_\alpha^{jk} = w_k^{-1} N^{-1} \sum_{l=0}^{N-1} (T_j \mathcal{L} T_k)(\cos \frac{(2l+1)\pi}{2N}) + \mathcal{O}(e^{-R_{\max} N}).$$

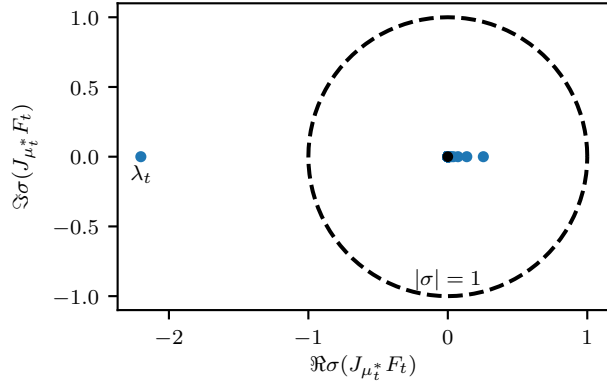


Figure 3: In blue, the spectrum of F_t 's fixed point's differential $D_{\mu_t^*} F_t$ for $t = 2.8$, as computed using `Poltergeist.jl`.

These sums themselves may be computed for all $j < N$ very quickly using the fast Fourier transform. Further details may be found in [45].

In practice, we note that when simulating the F dynamics acting on a specific function h , it is often more efficient to approximate the action of F directly

$$F(h) \approx P_n(\mathcal{L}_\alpha h)$$

rather than constructing a numerical representation of the operator $P_n \mathcal{L}_\alpha$ and applying it to h .

5 Numerically obtaining the homoclinic

Given that we can compute that action and derivatives of the thermodynamic limit map F_t to high accuracy, it then remains to present a method to compute other dynamical objects associated with the thermodynamic limit. In this section, these objects and the methods to compute them are described, starting from the unstable fixed point (Section 5.1), through its local manifold approximations (Section 5.2) to the homoclinic tangency itself (Section 5.2).

5.1 Hyperbolic fixed point

For $t \in [20, 40]$ the thermodynamic limit system F_t given in (6) has a fixed point μ_t^* with $\Phi_t^* := \varphi[\mu_t^*]$. If we define $\mu_{\text{acim}}(\alpha)$ to be the invariant probability density of transfer operator \mathcal{L}_α , then this can be computed numerically³ simply

³By considering the spectrum of the differential of F at the fixed point (see Figure 3), one may see that also be computed iteratively as a stable fixed point of the iteration $\mu_{n+1}^* =$

as $\mu_t^* = \mu_{\text{acim}}(t\Phi_t^*)$ where Φ_t^* solves

$$\Phi_t^* = \varphi[\mu_{\text{acim}}(t\Phi_t^*)].$$

At μ_t^* the Jacobian of F_t is given by

$$D_{\mu_t^*} F_t \psi = \mathcal{L}_{t\Phi_t^*} \psi - \psi t \mathcal{L}_{t\Phi_t^*} \partial_q X_{t\Phi_t^*}, \quad (9)$$

where X_α is defined in Appendix A so that

$$f_{\alpha+\epsilon} = f_\alpha + \epsilon X_\alpha \circ f_\alpha + \mathcal{O}(\epsilon^2). \quad (10)$$

Because our F_t dynamics are restricted to probability densities, we restrict the operator DF_t to functions of zero mean. Under this restriction, $D_{\mu_t^*} F_t$ is hyperbolic in the sense of having spectrum uniformly bounded away from the unit circle. In particular, its spectrum outside the unit disc consists of a single eigenvalue $\lambda_t < -1$ (see Figure 3). This unstable eigenvalue has right eigenfunction $e_t^u \in H_\rho$ and left eigenfunctional $d_t^u \in H_\rho^*$. We normalise e_t^u so that $\|e_t^u\|_{L^2_{\text{Cheb}}} = 1$ with $\langle 1, e_t^u \rangle_{\text{Cheb}} > 0$, and we normalise d_t^u to have $d_t^u e_t^u = 1$. We estimate these quantities to near-floating point precision very easily using the Chebyshev spectral methods in Section 4. In the case of e_t^u this may be done adaptively using `Poltergeist.jl`.

5.2 Local manifold approximations

The fixed point's unstable manifold $\mathcal{V}^u(\mu_t^*)$, which we write for short as \mathcal{V}_t^u , is parametrised near μ_t^* by

$$\mathcal{V}_t^u(a) = \mu_t^* + e_t^u a + \frac{1}{2} h_t^u a^2 + \mathcal{O}(a^3). \quad (11)$$

where the second-order correction is

$$h_t^u = (\lambda_t^2 - D_{\mu_t^*} F_t)^{-1} H_{\mu_t^*} F_t(e_t^u, e_t^u).$$

The tensor $H_{\mu_t^*} F_t$ is the Hessian of F_t at μ_t^* , with an explicit formula given in Appendix A. Like e_t^u , the function h_t^u is also easy to accurately approximate with spectral methods.

The parametrisation (11) has the useful property that $F_t(\mathcal{V}_t^u(a)) = F_t(\mathcal{V}_t^u(\lambda_t a))$. Furthermore, the tangent vectors to $\mathcal{V}_t^u(a)$ are generated by

$$(\mathcal{V}_t^u)'(a) = e_t^u + h_t^u a + \mathcal{O}(a^2). \quad (12)$$

At each point $\mathcal{V}_t^u(a)$ in the unstable manifold, this tangent vector generates its unstable subspace $E_{\mathcal{V}_t^u(a)}^u$.

On the other hand, the fixed point's local stable manifold $p \in \mathcal{V}^{s,\epsilon}(\mu_t^*)$, which we write for short as \mathcal{V}_t^s , is close to the kernel of the functional d_t^u , so that for $\mu \in \mathcal{V}^{s,\epsilon}(\mu_t^*)$,

$$d_t^u(\mu - \mu_t^*) = \mathcal{O}(\|\mu - \mu_t^*\|^2), \quad (13)$$

$$\overline{\frac{2}{3} F^t(\mu_n^*) + \frac{1}{3} F^t(F^t(\mu_n^*))}.$$

for $\mu \in \mathcal{V}_t^s$. We expect that, for all local stable points $\mu \in \mathcal{V}^{s,\epsilon}(\mu_t^*)$ and stable tangent vectors $v \in T_\mu \mathcal{V}_t^s$, the tangent hyperplanes to such an $\mathcal{V}^{s,\epsilon}(\mu_t^*)$ satisfy

$$d_t^u v = \mathcal{O}(\|\mu\|) \|v\|. \quad (14)$$

They constitute the stable subspace $E_{t,\mu}^s$ for $\mu \in \mathcal{V}_t^{s,\epsilon}$.

All these quantities can also be accurately estimated via spectral methods. They converge exponentially to the true estimates in the Hardy space H_R for certain $R > 0$, except notably for the leading left eigenfunctional d_t^u of $D_{\mu_t^*} F_t$ at the fixed point, which will converge exponentially in the dual space H_r^* for small $r \in (0, R)$.

We used the Julia package `Poltergeist.jl` to make and adaptively choose the order of the estimates [45]. The exception again is the left eigenfunctional d_t^u , which we computed iteratively via applying \mathcal{L}^* to a vector of Chebyshev coefficients until convergence was attained. The order of this approximation (*i.e.* the number of Chebyshev coefficients used) was chosen to be approximately that used by `Poltergeist.jl` for estimating the right eigenfunctions⁴

5.3 Shooting method

Our aim is to find a parameter t and a point $q \in \mathcal{V}_t^u$ such that $q \in \mathcal{V}_t^s$ also, with unstable subspace $E_{t,q}^u$ a subset of the stable subspace $E_{t,q}^s$. Because we have good knowledge of the local stable and unstable manifolds near fixed points μ_t^* , we rephrase this as attempting to find a pair (t, a) such that

$$F_t^n(\mathcal{V}_t^u(a)) \rightarrow \mu_t^*, \quad (H1)$$

$$(D_{\mathcal{V}_t^u(a)} F_t^n)(\mathcal{V}_t^u)'(a) \rightarrow 0. \quad (T1)$$

Since $F_t^n(\mathcal{V}_t^u(a))$ converges towards μ_t^* , we can use the local linearisation of the stable manifold (13) and (H1–T1) becomes equivalent to solving

$$d_t^u(F_t^n(\mathcal{V}_t^u(a)) - \mu_t^*) \rightarrow 0, \quad (H2)$$

$$d_t^u(D_{\mathcal{V}_t^u(a)} F_t^n)(\mathcal{V}_t^u)'(a) \rightarrow 0, \quad (T2)$$

where now the left-hand quantities are one-dimensional instead of lying in a Banach space H_r as before.

It turns out that a numerically stable way to satisfy these conditions is for each t to find $a(t)$ satisfying (T2), followed by optimising t to satisfy (H2). In both cases, because of the finite precision of floating-point arithmetic, and because μ_t^* is a saddle, we will not in practice be able to compute an orbit converging to μ_t^* by simple shooting. Instead, we must assume that the convergence holds along the orbit up until some $n = n_*$ determined by the floating-point precision.

⁴At higher numerical precisions it was also most efficient here to compute eigendata iteratively via the power method, using `Poltergeist.jl` to compute the action of $D_{\mu_t^*} F_t$ on an eigenvector estimate, renormalising and so on.

We eventually chose our floating-point precision to be 159 bits (*i.e.* three times as many bits as the standard double precision), using the GNU MPFR library implemented as the `BigFloat` type in Julia. Having refined our guess progressively at lower precisions, as bracketing intervals we chose

$$a \in 0.792\,760\,229\,502\,464\,90 + [0, 2 \times 10^{-17}]$$

$$t \in 2.786\,033\,304\,650\,978\,791 + [0, 2 \times 10^{-18}].$$

To compute $q_t = \mathcal{V}_t^u(a)$ accurately we apply the approximation (11) to $f^{-n_\epsilon}(q_t) = \mathcal{V}_t^u(\lambda^{-n_0}a)$, where we choose $n_0 = \lceil \log_{2.19}(\epsilon^{-1/3}) \rceil = 16$, where $\epsilon \approx 2.7 \times 10^{-48}$ is the relative accuracy of the floating-point encoding. Because $\lambda_t \approx -2.19$ for $t \approx 30$, this gives us an error $|f^{-n}(q_t) - \mu_t^*| = \mathcal{O}(\epsilon^{2/3})$. Because we are shrinking our starting point by $\mathcal{O}(\epsilon^{1/3})$, it also gives us an effective numerical precision of $\mathcal{O}(\epsilon^{2/3})$ rather than the full $\mathcal{O}(\epsilon)$.

To estimate the tangent vector at q , $(\mathcal{V}_t^u)'(a)$, we estimate

$$(\mathcal{V}_t^u)'(a) = \lambda_t^{-2n_0} \left(D_{\mathcal{V}_t^u(\lambda_t^{-n_0}a)} F_t^{n_0} \right) \left(D_{\mathcal{V}_t^u(\lambda_t^{-2n_0}a)} F_t^{n_0} \right) (\mathcal{V}_t^u)'(\lambda_t^{-2n_0}a)$$

where \mathcal{V}_t^u and its derivative are computed using (12) when they are evaluated at $\lambda_t^{-2n_0}a$. This also returns an error of $\mathcal{O}(\epsilon^{2/3})$.

For fixed $n = n_1$, the left-hand sides of (H2) and (T2) are monotone in a and t over sufficiently small intervals. We therefore fixed n in these two equations and used interval subdivision over parameters of t to find $(t, a(t))$ satisfying (H2), where for each t we found (again by subdivision) $a(t)$ satisfying (T2).

We fixed $n_1 = 5 + \lceil \log_{2.19 \times 0.255^{-2}} \epsilon^{-2/3} \rceil = 12$, which is approximately when we expect the quantities in (H2) and (T2) to reach their minimum within the bounds of our numerical precision. This choice can be explained as follows. The homoclinic orbit $F^n(\mathcal{V}_t^u(a))$ approaches μ_t^* as $\mathcal{O}(\tilde{\lambda}_t^n)$, where $\tilde{\lambda}_t \approx 0.255$ is the spectral radius of the fixed point differential $D_{\mu_t^*} F$ in the stable subspace. Because d_t^n captures the local stable manifold of μ_t^* to first order, it has a second-order error in the distance to the fixed point, and so the quantities in (H2) and (T2) decay as $\mathcal{O}(0.255^{2n})$. On the other hand, the initial error grows as $\mathcal{O}(\epsilon^{2/3} \lambda_t^n)$. This halts the decay of the quantities we are interested in at $n \approx n_1$, and the magnitudes of these quantities bottom out at $\epsilon^{2/3(1+\log 0.255^{-1}/2 \log 2.19)} = 3 \times 10^{-20}$.

Our shooting method (as well as routines to compute stable and unstable manifolds in extended floating point) is contained in the supplementary file `quadratic3.jl`.

6 Results

We can now present the results we used to compute these quantities.

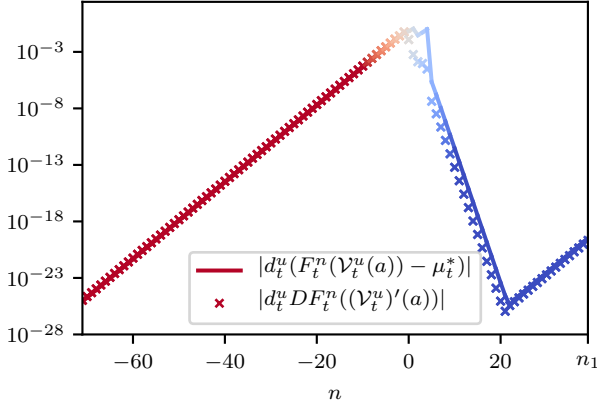


Figure 4: The distance (H2) from points along the numerical approximation of the homoclinic orbit to the linearised stable manifold of $\mu_{t_{ht}}^*$ (line), and the size(T2) of the corresponding covariant unstable vector's component in the unstable direction of $\mu_{t_{ht}}^*$ (crosses).

6.1 Existence of a homoclinic tangency

Using the shooting method we obtained the following (non-rigorously validated) estimates for the parameters of a homoclinic tangency:

$$t_{ht} = 2.786\,033\,304\,650\,978\,792\,184\,539\,709\,484\,2 \pm 2 \times 10^{-31}$$

$$a_{ht} = 0.792\,760\,229\,502\,464\,909\,617\,483\,088\,582\,5 \pm 2 \times 10^{-31}.$$

The relevant homoclinic orbit is plotted with its unstable vectors in Figure 6, and the quantities (H2–T2) we aimed to minimise are plotted in Figure 4. In Figure 5 we verify that the original homoclinic tangency conditions (H1–T1) are also satisfied.

The precision achieved in these estimates is of a comparable $\epsilon^{2/3} = 2 \times 10^{-32}$ error with our 159-bit floating point precision. The quantities in (H2) and (T2) reach their minima a little before $n = n_1 = 62$, as predicted, and these minima are of the order of $\epsilon^{2/3(1+\log 0.255^{-1}/2\log 2.19)} = 8 \times 10^{-21}$, also as predicted.

These results are obtained to a high precision, with all apparent errors being of the predicted order. Because the thermodynamic limit system F_t has very high regularity with strong compactness properties, it is therefore essentially guaranteed that such a homoclinic tangency exists.

We also have evidence that the homoclinic tangency is generic in two ways that together suggest persistent wild, non-hyperbolic behaviour under perturbation [6].

Firstly, the homoclinic tangency is quadratic, that is to say that the tangency between the stable and unstable manifolds is a quadratic tangency. The

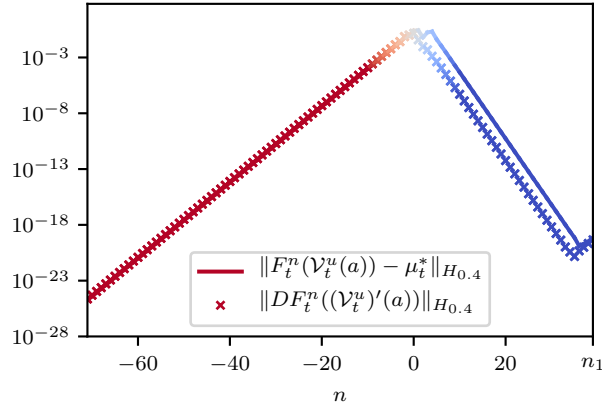


Figure 5: The distance from the numerical approximation of the homoclinic orbit to the fixed point (line), and of the norm of the unstable vector pushed forward under the orbit (crosses).

functional d_t^u measures the distance to the local stable manifold of μ_t^* (to first order in the distance from μ_t^*): in Figure 7 we plot the distances to the unstable manifold at $F_{t_{\text{ht}}}^n(\mathcal{V}_{t_{\text{ht}}}^u(a))$ for $a \approx a_{\text{ht}}$, as well as the derivative of this with respect to a . The derivative is smooth and clearly has non-zero slope at $a = a_{\text{ht}}$, meaning the tangency is quadratic. This could be explicitly demonstrated in future work by showing $\frac{d^2}{da^2} F_{t_{\text{ht}}}^{n_1}(\mathcal{V}_{t_{\text{ht}}}^u(a)) \neq 0$.

Secondly, we also have strong evidence that tangency is perturbed generically, in the sense that for all t slightly less than t_{ht} the unstable manifold around the homoclinic orbit is locally separated from the stable manifold (see Figure 8). In fact, as we might expect, the displacement of the unstable manifold as t is varied is linear and transversal to the stable manifold. If our system was a diffeomorphism, satisfaction of these criteria for a quadratic tangency would imply the existence of heteroclinic tangencies (*i.e.* non-hyperbolicity) on an open set of parameters t [32, 34].

To this end, we find that at $t = t_{\text{ht}}$ we find that the fixed point is *sectionally dissipative*: the differential of the fixed point has leading eigenvalue $\lambda_t < -1.9898$ and all other eigenvalues having modulus less than $0.255 < |-1.9818|^{-1}$, meaning that any product of two eigenvalues has modulus less than one. As a result, we can also expect a Baire generic Cantor set of parameters t where an infinite number of stable periodic orbits coexist [34, 7].

6.2 Dynamics at $t = t_{\text{ht}}$

Although we have that the map F_t is non-hyperbolic, Hypothesis 1 applies only to dynamics on the attractor of the system, which is to say, presumably, on the attractor of the macroscopic dynamics. We therefore wish to have some idea

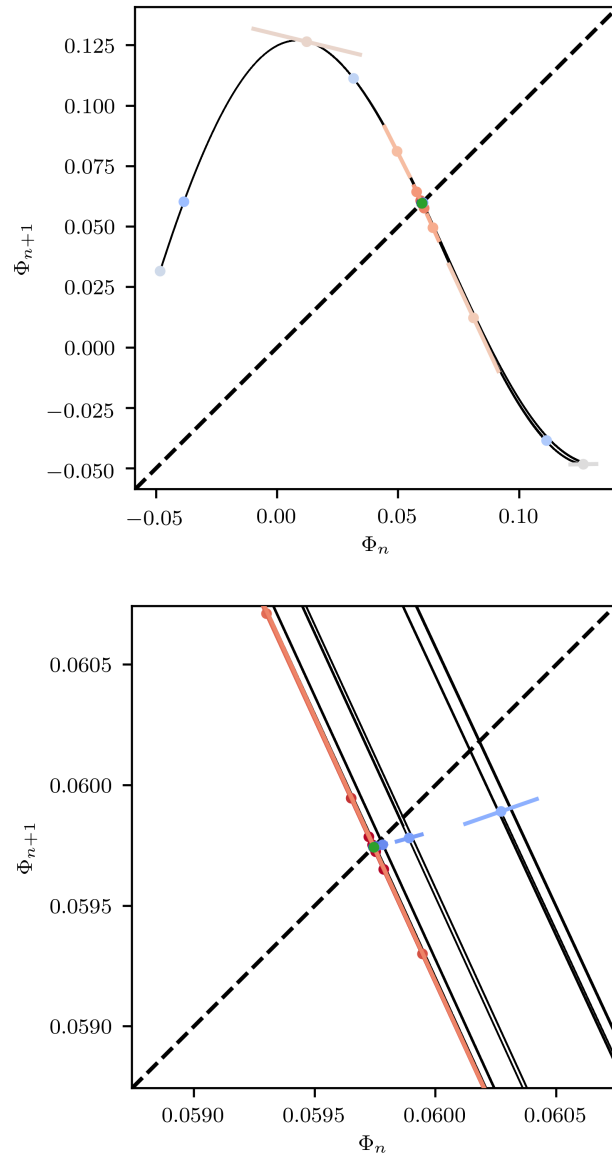


Figure 6: Top: plot of the homoclinic orbit and its covariant unstable vectors, in the same colours as in Figures 5–4, projected onto delay coordinates in the mean-field Φ_n . The attractor of the F dynamics is plotted in black, and the fixed point μ_{ht}^* is plotted as a green dot.
 Bottom: detail near the fixed point. The leading stable eigenvalues of the differential of F at the fixed point μ_{ht}^* are complex (see Figure 3), causing the spiralling behaviour of the homoclinic orbit seen here.

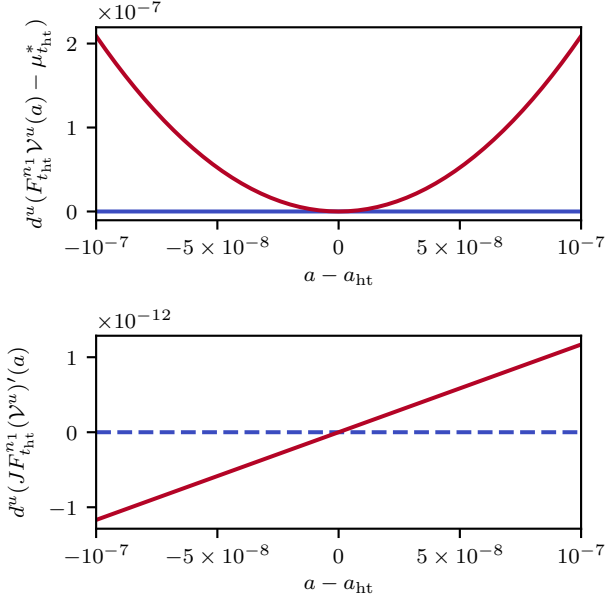


Figure 7: Top: the unstable manifold near the homoclinic orbit point $F^{n_1}(\mathcal{V}_{t_{ht}}^u(a_{ht}))$ (red) and the linearised stable manifold (blue). These are projected into one dimension using the eigenfunctional $d_{t_{ht}}^u$. Bottom: the derivative of the unstable manifold near the homoclinic orbit point $\frac{d}{da} F^{n_1}(\mathcal{V}_{t_{ht}}^u(a_{ht}))$ (red) and the linearised stable manifold (blue), again similarly projected.

of the macroscopic dynamics's attractor, and in particular whether homoclinic tangency lies on it.

We simulated the thermodynamic limit dynamics at $t = t_{ht}$ using `Poltergeist.jl` [47, Appendix B]. The dynamics is chaotic: through simulations on 10 time series of 10^4 realisations we estimated the leading Lyapunov exponents as $\lambda_1 = 0.381 \pm 0.005 > 0$, $\lambda_2 = -1.150 \pm 0.003 < 0$, $\lambda_3 = -2.015 \pm 0.004 < 0$. This implies the attractor has dimension at least 1, and in particular that its Kaplan-Yorke dimension 1.249 ± 0.002 . The dynamics also appears to be exponentially mixing over timescale $t_{1/e} \approx 9$.

Under this assumption that the attractor is chaotic, there is substantial evidence that the fixed point's unstable manifold, and hence the homoclinic orbit actually lies on this attractor. In Figure 6 it is clear that the attractor contains long unstable manifolds that pass near the fixed point in a direction generally parallel to the unstable vector of the fixed point. We therefore expect that these unstable manifold must have intersections with the stable manifold of the fixed point, implying that the fixed point lies on the attractor. To support this, in Figure 9, we show that μ_t^* is separated from the F_t -attractor by at most

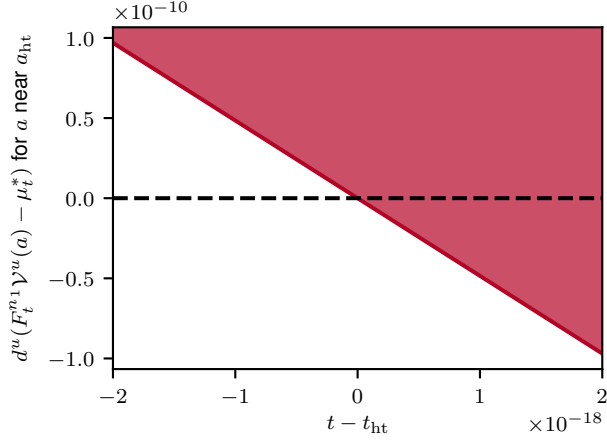


Figure 8: In block colour, the displacement from the local unstable manifold to the local stable manifold at $F_t^{n_1}(\mathcal{V}_t^u(a))$ for $a \approx a_{ht}$ and $t \lesssim t_{ht}$, projected into real coordinates using d_t^u . As a line, the minimum value attained for given t .

4×10^{-6} in $W^{2,1}$ distance, and furthermore that there is a regular scaling of the physical measure of the F_t dynamics as the distance from the fixed point tends to zero, suggesting that μ_t^* lies in its support.

Because the attractor contains the fixed point and the system is chaotic (so cannot be confined to the stable manifold of the fixed point), the attractor must also contain the unstable manifold of the fixed point and thus the homoclinic tangency. As a consequence, we can conclude that, not just the map F , but the actual *large-scale dynamics on the attractor* are non-hyperbolic. This is in contradiction of Hypothesis 1.

7 Conclusion

The chaotic hypothesis (Hypothesis 1) makes a broad claim about the large-scale behaviour of complex chaotic systems. This paper provides a counterexample to it in a mean-field coupled system. We studied this system's thermodynamic limit, which encodes the large-scale dynamics and which the chaotic hypothesis therefore predicts to be hyperbolic on its attractor. We have found however that this attractor contains a homoclinic tangency, and the dynamics on it therefore are non-hyperbolic.

On the other hand, a commonly cited restriction on Hypothesis 1 is that it holds only for *generic* systems: thus, the homoclinic tangency we find could be a special point. However, as a result of having certain genericity properties discussed in Section 6.1, our homoclinic tangency can be expected to generate

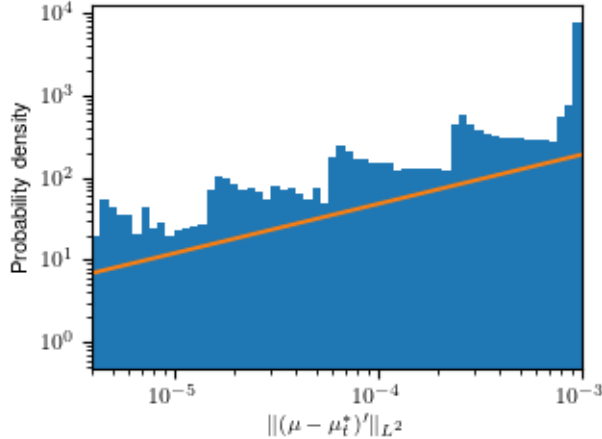


Figure 9: In blue, a histogram of the $W^{2,1}$ distance from fixed point μ_t^* in the attracting F_t -dynamics. In orange, a logarithmic slope of gradient 0.6, indicating a local fractal dimension of around 1.6 for the SRB measure of F_t at the fixed point. The histogram was obtained from a single time series μ_n of which 400,000 timesteps had $d_{W^{2,1}}(\mu_n, \mu_t^*) \leq 0.003$.

Here we let the $W^{2,1}$ distance between two mean-zero probability densities μ, ν be $\|\partial_x(\mu - \nu)\|_{L^2}$. This is equivalent to the $W^{2,1}$ Sobolev norm, in which our transfer operators are quasi-compact. However, this distance is faster to compute than the Hardy norms.

non-hyperbolic structures on an open set of parameters, following a result of [34]. This results state that for C^∞ diffeomorphisms with one unstable direction but perhaps infinite stable directions, these genericity properties imply the existence of heteroclinic tangencies between stable and unstable manifolds of (non-fixed) hyperbolic points, on an open set of nearby parameters [34]. While our system is not a diffeomorphism, this arises because of very strong stable contracting directions and so fits the spirit of the result. Thus, as well as having a non-hyperbolic system at one parameter $t = t_{\text{ht}}$, we in fact expect non-hyperbolicity on an interval of parameters.

Furthermore, homoclinic tangencies can birth a wide array of exotic objects [8, 30, 48, 34]. Of particular note is the Newhouse phenomenon, where infinitely many sinks may coexist in a single system: because the fixed point of the homoclinic tangency is sectionally dissipative, this peculiar phenomenon occurs on a Baire generic⁵ set of parameters t [34, 31]. It is a curiosity therefore that for these Newhouse parameters, it is impossible to sample all possible (if unlikely) attracting dynamics. On the other hand, passing from the thermodynamic

⁵A Baire generic set is the countable intersection of open dense sets. For diffeomorphisms of two-dimensional manifolds, the Hausdorff dimension of the set of Newhouse parameters is at least 1/2 [7] and is conjectured to be of measure zero [33].

limit back to finite ensemble size M introduces a small Gaussian noise that will immediately break such dynamical structures.

Although they demonstrate a kind of generic non-hyperbolicity in globally coupled systems, these coupled systems are somewhat atypical of many real-world systems in the sense that they have a uniform all-to-all network structure. In many more realistic systems such as in geophysics, interactions may be spatially localised, and separation between spatial scales may be incomplete. In such systems, emergent noise that forms the first-order correction to the thermodynamic limit may lead to large-scale *stochastic* dynamics [46, 47], which share many helpful similarities with hyperbolic dynamics [49]. Furthermore, even in a globally-coupled systems, physically meaningful coupling types such as attractive or repulsive behaviours may impose their own dynamical constraints which preclude non-hyperbolic behaviour [23]. Nonetheless, our results show that one cannot guarantee “nice” large-scale dynamics: these depend on the structure of the complex system.

Acknowledgements

This research has been supported by the European Research Council (ERC) under the European Union’s Horizon 2020 research and innovation programme (grant agreement No 787304).

The author thanks Roberto Castorrini for his comments on the manuscript.

A Appendix

The perturbation function of f_α as defined in (10) is given explicitly by

$$X_\alpha(q) = g'(\alpha)(1 - \mathfrak{d}(f^{-1}(q))^2) = g'(\alpha) \left(1 - \left(\frac{2(q - g(\alpha))}{1 + \sqrt{1 - 4g(\alpha)(q - g(\alpha))}} \right)^2 \right)$$

Let $X_\alpha^{(1)} := \frac{\partial X_\alpha}{\partial \alpha}$ be its derivative with respect to α .

If we define the operator $\Gamma_t(\mu) := \mathcal{L}_{t\varphi[\mu]}$ then we have $F_t(\mu) = \Gamma_t(\mu)\mu$. It is standard [1] that

$$D_\mu \Gamma_t(v) = \varphi[v] \partial_q X_{t\varphi[\mu]} \Gamma_t(\mu)$$

and by recursion, the Hessian

$$H_\mu \Gamma_t(v, w) = \varphi[v] \partial_q \left(X_{t\varphi[\mu]}^{(1)} \Gamma_t(\mu) + X_{t\varphi[\mu]} D_\mu \Gamma_t[v] \right).$$

As a result, the differential of F is given by

$$(D_\mu F_t)(v) = \Gamma_t(\mu)v + D_\mu \Gamma_t(v)\mu$$

and the Hessian is given by

$$(H_\mu F_t)(v, w) = D_\mu \Gamma_t(v + w)\mu + H_\mu \Gamma_t(v, w)\mu.$$

References

- [1] V. BALADI, *Linear response, or else*, in ICM Seoul 2014, Proceedings, Volume III, Aug 2014, pp. 525–545.
- [2] V. BALADI, *Dynamical Zeta Functions and Dynamical Determinants for Hyperbolic Maps*, Springer, Berlin, 2016.
- [3] V. BALADI, M. BENEDICKS, AND D. SCHNELLMANN, *Whitney–Hölder continuity of the SRB measure for transversal families of smooth unimodal maps*, *Inventiones mathematicae*, 201 (2015), pp. 773–844.
- [4] O. F. BANDTLOW AND J. SLIPANTSCHUK, *Lagrange approximation of transfer operators associated with holomorphic data*, arXiv preprint arXiv:2004.03534, (2020).
- [5] T. L. BELL, *Climate sensitivity from fluctuation dissipation: Some simple model tests*, *Journal of the Atmospheric Sciences*, 37 (1980), pp. 1700–1707.
- [6] P. BERGER, *Generic family with robustly infinitely many sinks*, *Inventiones mathematicae*, 205 (2016), pp. 121–172.
- [7] P. BERGER AND J. DE SIMOI, *On the Hausdorff dimension of Newhouse phenomena*, in *Annales Henri Poincaré*, vol. 17, Springer, 2016, pp. 227–249.
- [8] C. BONATTI AND L. J. DÍAZ, *Persistent nonhyperbolic transitive diffeomorphisms*, *Annals of Mathematics*, 143 (1996), pp. 357–396.
- [9] F. BONETTO, G. GALLAVOTTI, A. GIULIANI, AND F. ZAMPONI, *Chaotic hypothesis, fluctuation theorem and singularities*, *Journal of Statistical Physics*, 123 (2006), p. 39.
- [10] R. BOWEN, *Equilibrium states and the ergodic theory of Anosov diffeomorphisms*, Lecture notes in mathematics, 470, Springer, Berlin, 2nd ed., 2008.
- [11] J.-R. CHAZOTTES AND B. FERNANDEZ, *Dynamics of coupled map lattices and of related spatially extended systems*, vol. 671, Springer Science & Business Media, 2005.
- [12] M. D. CHEKROUN, J. D. NEELIN, D. KONDRASHOV, J. C. MCWILLIAMS, AND M. GHIL, *Rough parameter dependence in climate models and the role of Ruelle-Pollicott resonances*, *Proceedings of the National Academy of Sciences*, 111 (2014), pp. 1684–90.
- [13] F. COOPER AND P. HAYNES, *Assessment of the fluctuation-dissipation theorem as an estimator of the tropospheric response to forcing*, *Quart. J. Roy. Met. Soc.*, (2013). Submitted.

- [14] D. FUCHS, S. SHERWOOD, AND D. HERNANDEZ, *An exploration of multivariate fluctuation dissipation operators and their response to sea surface temperature perturbations*, Journal of the Atmospheric Sciences, 72 (2014), pp. 472–486.
- [15] S. GALATOLLO, *Self consistent transfer operators in a weak coupling regime. invariant measures, convergence to equilibrium, linear reponse and control of the statistical properties*, arXiv preprint arXiv:2105.12388, (2021).
- [16] G. GALLAVOTTI, *Nonequilibrium and fluctuation relation*, arXiv preprint arXiv:1906.10069, (2019).
- [17] G. GALLAVOTTI AND E. G. D. COHEN, *Dynamical ensembles in nonequilibrium statistical mechanics*, Phys. Rev. Lett., 74 (1995), pp. 2694–2697.
- [18] ———, *Dynamical ensembles in stationary states*, Journal of Statistical Physics, 80 (1995), pp. 931–970.
- [19] A. GRITSUN, *Statistical characteristics, circulation regimes and unstable periodic orbits of a barotropic atmospheric model*, Philosophical Transactions of the Royal Society A: Mathematical, Physical and Engineering Sciences, 371 (2013), p. 20120336.
- [20] K. KANEKO, *Self-consistent Perron-Frobenius operator for spatiotemporal chaos*, Physics Letters A, 139 (1989), pp. 47–52.
- [21] ———, *Globally coupled chaos violates the law of large numbers but not the central-limit theorem*, Physical review letters, 65 (1990), p. 1391.
- [22] G. KELLER, *An ergodic theoretic approach to mean field coupled maps*, in Fractal geometry and stochastics II, Springer, 2000, pp. 183–208.
- [23] J. KOILLER AND L.-S. YOUNG, *Coupled map networks*, Nonlinearity, 23 (2010), p. 1121.
- [24] S. P. KUZNETSOV, *Possible occurrence of hyperbolic attractors*, in Hyperbolic Chaos, Springer, 2012, pp. 35–56.
- [25] J. L. LEBOWITZ AND H. SPOHN, *A Gallavotti–Cohen-type symmetry in the large deviation functional for stochastic dynamics*, Journal of Statistical Physics, 95 (1999), pp. 333–365.
- [26] V. LEMBO, V. LUCARINI, AND F. RAGONE, *Beyond forcing scenarios: Predicting climate change through response operators in a coupled general circulation model*, arXiv preprint arXiv:1912.03996, (2019).
- [27] S. LEPRI, R. LIVI, AND A. POLITI, *Energy transport in anharmonic lattices close to and far from equilibrium*, Physica D: Nonlinear Phenomena, 119 (1998), pp. 140–147.

- [28] V. LUCARINI, D. FARANDA, J. WOUTERS, AND T. KUNA, *Towards a general theory of extremes for observables of chaotic dynamical systems*, Journal of statistical physics, 154 (2014), pp. 723–750.
- [29] A. J. MAJDA, R. ABRAMOV, AND B. GERSHGORIN, *High skill in low-frequency climate response through fluctuation dissipation theorems despite structural instability*, Proceedings of the National Academy of Sciences, 107 (2010), pp. 581–586.
- [30] L. MORA AND M. VIANA, *Abundance of strange attractors*, Acta mathematica, 171 (1993), pp. 1–71.
- [31] S. E. NEWHOUSE, *Diffeomorphisms with infinitely many sinks*, Topology, 13 (1974), pp. 9–18.
- [32] ———, *The abundance of wild hyperbolic sets and non-smooth stable sets for diffeomorphisms*, Publications Mathématiques de l’IHÉS, 50 (1979), pp. 101–151.
- [33] J. PALIS, *Open questions leading to a global perspective in dynamics*, Nonlinearity, 21 (2008), pp. 1–37.
- [34] J. PALIS AND M. VIANA, *High dimension diffeomorphisms displaying infinitely many periodic attractors*, Annals of mathematics, (1994), pp. 207–250.
- [35] A. S. PIKOVSKY AND J. KURTHS, *Do globally coupled maps really violate the law of large numbers?*, Phys. Rev. Lett., 72 (1994), pp. 1644–1646.
- [36] F. RAGONE, V. LUCARINI, AND F. LUNKEIT, *A new framework for climate sensitivity and prediction: a modelling perspective*, Climate Dynamics, 46 (2016), pp. 1459–1471.
- [37] D. RUELLE, *Differentiation of SRB states*, Communications in Mathematical Physics, 187 (1997), pp. 227–241.
- [38] ———, *Linear response theory for diffeomorphisms with tangencies of stable and unstable manifolds—a contribution to the Gallavotti-Cohen chaotic hypothesis*, Nonlinearity, 31 (2018), p. 5683.
- [39] E. SANDER, *Homoclinic tangles for noninvertible maps*, Nonlinear Analysis: Theory, Methods & Applications, 41 (2000), pp. 259–276.
- [40] J. SEDRO, *A regularity result for fixed points, with applications to linear response*, Nonlinearity, 31 (2018), p. 1417.
- [41] F. M. SÉLLEY, *A self-consistent dynamical system with multiple absolutely continuous invariant measures*, arXiv preprint arXiv:1909.04484, (2019).

- [42] F. M. SÉLLEY AND M. TANZI, *Linear response for a family of self-consistent transfer operators*, Communications in Mathematical Physics, 382 (2021), pp. 1601–1624.
- [43] L. N. TREFETHEN, *Approximation theory and approximation practice*, Siam, Philadelphia, PA, 2013.
- [44] C. L. WORMELL, *Poltergeist*, 2017. Available at <https://github.com/wormell/Poltergeist.jl> and in the Julia package repository.
- [45] ———, *Spectral Galerkin methods for transfer operators in uniformly expanding dynamics*, Numerische Mathematik, 142 (2019), pp. 421–463.
- [46] C. L. WORMELL AND G. A. GOTTWALD, *On the validity of linear response theory in high-dimensional deterministic dynamical systems*, Journal of Statistical Physics, 172 (2018), pp. 1479–1498.
- [47] C. L. WORMELL AND G. A. GOTTWALD, *Linear response for macroscopic observables in high-dimensional systems*, Chaos: An Interdisciplinary Journal of Nonlinear Science, 29 (2019), p. 113127.
- [48] J. A. YORKE AND K. T. ALLIGOOD, *Cascades of period-doubling bifurcations: a prerequisite for horseshoes*, Bulletin (New Series) of the American Mathematical Society, 9 (1983), pp. 319–322.
- [49] L.-S. YOUNG, *Comparing chaotic and random dynamical systems*, Journal of Mathematical Physics, 60 (2019), p. 052701.